Chapter 7

SCALAR COUPLING

Scalar couplings arise from spin-spin interactions that occur via bonding electrons. Consequently, they provide information on the chemical *connectivity* between atoms. Therefore, these couplings can be utilized to correlate NMR signals of atoms that are chemically bonded to one another, providing chemical shift assignments if the molecular structure is known. In particular, the scalar coupling across the peptide bond permits the linkage of spins within one amino acid to those of its neighbors, as discussed in Chapter 13.

In addition to providing information on chemical connectivities, the sizes of three bond scalar couplings are sensitive to the electron distribution of the intervening bonds, consequently these couplings can provide information on the conformation of rotatable bonds in proteins.

In this chapter we will first explore the origin of scalar couplings between nuclear spins, understanding the effect of this coupling on the resultant NMR spectrum from a classical perspective. The coupling will then be analyzed using quantum mechanics to fully evaluate the effect of the coupling on the frequency and intensity of resonance lines in the NMR spectrum of coupled spins. Finally, a density matrix treatment of coupled spins will be introduced in the subsequent Chapter as a prelude to analyzing the effect of scalar coupling in more complex multi-dimensional NMR spectra.

7.1 Introduction to Scalar Coupling

Scalar, or J-coupling, occurs between nuclei which are connected by chemical bonds. This coupling causes splitting of the spectral lines for both coupled spins by an amount J, or the coupling constant (See Fig. 7.1). The nomenclature that is used to describe the coupling is as follows:

$$^{n}J_{AB}$$

where n refers to the number of intervening bonds, and A and B identify the two coupled spins. For example, the coupling constant between the amide nitrogen and the C_β carbon would be written as: $^{2}J_{NC_\beta}$. The value of J is usually given in Hz and

is the observed frequency separation between the split resonance lines of the coupled spins (see below). A resonance line that is split due to J-coupling is generally referred to as a multiplet. The spectrum shown in Fig. 7.1 is an example of a doublet. If the resonance line was split into three signals, it would be called a triplet. Finally, splitting into four lines generates a quartet.

The effect of J-coupling on the spectrum depends on the frequency separation of the coupled spins. If the two coupled spins differ greatly in their resonance frequencies ($\Delta\nu > J$), then the system is referred to as an AX system, where the X signifies the fact that the two chemical shifts are quite different. All coupling between different atom types, or heteronuclear spins, are AX couplings because of the large difference in the frequencies of coupled spins. Examples include, J_{NH}, J_{CH}, and J_{NC}. AX couplings can be analyzed using a classical analysis, similar to that depicted in Fig. 7.1. When two coupling spins have nearly equivalent resonance frequencies ($\Delta\nu \leq J$) then the system is referred to as an AB system. For example, the coupling between two H_β protons on an amino acid is an example of an AB system. Accurate analysis of AB systems require a detailed quantum mechanical treatment. Lastly, when the coupled spins have the identical resonance frequencies, the observed coupling disappears entirely. This is most often seen when multiple protons have equivalent environments, such as the three protons on a methyl group.

7.2 Basis of Scalar Coupling

Scalar coupling arises from the interaction of the nuclear magnetic moment with the electrons involved in the chemical bond. The nuclear spin polarization of one atom affects the polarization of the surrounding electrons. The electron polarization subsequently produces a change in the magnetic field that is sensed by the coupled spin. For example, consider a C-H group in a molecule, as illustrated in Fig. 7.1. The proton nuclear spin polarizes the electron in the σ bonding orbital. This polarization alters the magnetic field at the carbon nucleus. Since there are two possible spin states for the proton magnetic dipole, the effective field at the carbon nucleus is increased

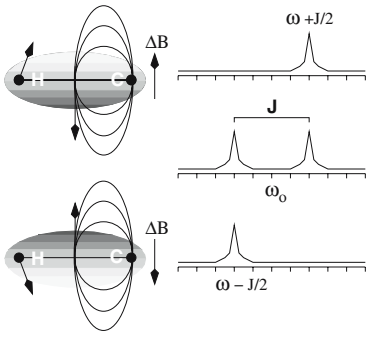

Figure 7.1 Nuclear spin coupling in a ^{13}C-H group. Two C-H groups in separate, but otherwise identical molecules, are shown. The two molecules differ only in the spin state of the proton. The bonding electrons in the σ orbital become polarized from the proton magnetic dipole, as indicated by the oval field lines. The polarization of the electrons can either increase or decrease the magnetic field at the ^{13}C nucleus, depending on the proton spin state. One orientation of the proton spin increases the magnetic field (upper molecule), while the other orientation causes a decrease in the apparent field (lower molecule), causing either an upfield or downfield shift in the resonance line, depending on the spin-state of the attached proton. The observed carbon spectrum is the sum of these two resonances, giving two peaks that are separated by the J-coupling constant, as shown in the middle spectrum.

or decreased, depending on the spin state of the attached proton. Since the population differences between the two orientations of the proton spin are approximately equal, one-half of the attached carbons will experience an increase in the local magnetic field while the other half will experience a decrease. This difference in the local magnetic field at the carbon nucleus will lead to a shift of the carbon resonance frequency. Since there are two possible proton spin states, the carbon spectrum is split into two lines, with the separation between the lines equal to the J-coupling.

The change in the magnetic field induced by the proton spins is proportional to γ_H. The corresponding change in the carbon resonance frequency is proportional to the product of this field change and the gyromagnetic ratio of the carbon spin, i.e.:

$$\Delta\omega \propto \pm\gamma_H\gamma_C \tag{7.1}$$

The effect of the carbon spin on the proton spin is calculated in the same way. The change in the local magnetic field at the proton nucleus is proportional to $\pm\gamma_C$, giving rise to a frequency shift of the protons of $\pm\gamma_C\gamma_H$. Consequently, the proton spin will experience exactly the same shift in frequency as its coupled partner, giving rise to exactly the same splitting of the proton resonance line as the resonance line from the attached carbon. Also note that the observed frequency shift only depends on the product of the gyromagnetic ratios of the coupled spins; the scalar coupling constant is independent of the applied magnetic field (B_o).

Values of J-coupling constants that are important in biomolecular NMR are shown in Table 7.1. The strength of the J-coupling depends on several factors, including the gyromagnetic ratio of the coupled spins, the number of bonds connecting the coupled spins, and the conformation of the intervening bonds in the case of multiple bond couplings. The series of single bond heteronuclear couplings (Table 7.1, left column) illustrates the effect of the gyromagnetic ratio on the coupling constant; the coupling constant increases with increasing γ. Scalar coupling through multiple bonds greatly attenuates the coupling. For example, the strong single bond H-C coupling of 130 Hz is reduced to 5 Hz when an additional carbon-carbon bond is inserted between the two coupled spins (Table 7.1).

In the case of multiple bond couplings, the conformation of the coupled atoms affects the coupling constant. For example, the three bond proton-proton coupling in

Table 7.1. Homonuclear and heteronuclear coupling constants. Homonuclear (proton-proton) and heteronuclear coupling constants that are commonly found in biopolymers are listed. The values in this table are approximate; the coupling constants will also be affected by the electronic environment of the associated spins.

Couplings Involving Heteronuclear (^{13}C or ^{15}N) Spins		*Proton-Proton Couplings*	
C-N	14 Hz	H-C-H	-12 to -15 Hz
C-C	35 Hz	H-C-C-H	2-14 Hz
H-N	92 Hz	H-C=C-H	10 (cis)/17 (trans)
H-C	130 Hz	H-N-C-H	1-10 Hz
H-C-C	5 Hz (two bond coupling)		(3 Hz α-helix)
			(10 Hz β-strand)

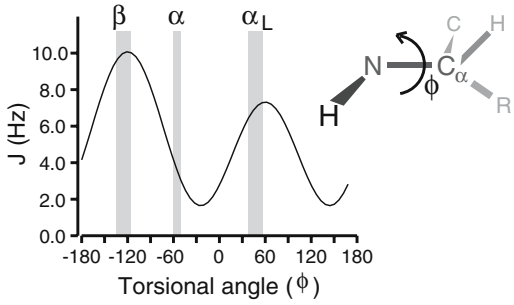

Figure 7.2 Karplus curve for a peptide group. The relationship between J and the ϕ torsional angle in polypeptides is shown. The ϕ angles for regular secondary structures are indicated by the vertical gray bars. The ϕ torsional angle is defined by the relative orientation of the H-N bond vector to the C_α-CO bond vector. The molecular fragment to the right of the plot has a ϕ angle of 180°. The actual curve plotted is: $J = 6.98\,cos^2(\phi - 60) - 1.38\,cos(\phi - 60) + 1.72$ (from Ref. [162]).

the H-C-C-H group ranges from 2 to 14 Hz. The relationship between the coupling constant and the torsional angle is represented by the Karplus relationship [80]:

$$J = Acos^2\theta + Bcos\theta + C \tag{7.2}$$

where A, B, and C are empirical constants. For example, the ϕ angle in the peptide bond affects the strength of the coupling between the amide proton and the alpha proton, as illustrated in Fig. 7.2.

7.2.1 Coupling to Multiple Spins

The coupling between a carbon and a hydrogen in a ^{13}C-H group results in the splitting of both the proton and carbon spectral line by an amount J_{CH} Hz. If the carbon atom is coupled to more than one *equivalent* proton[1], such as in a $^{13}CH_2$ or $^{13}CH_3$ group, then a more complex splitting pattern is observed.

In the case of a $^{13}CH_2$ group a triplet of lines is observed in the carbon NMR spectrum, as illustrated in Fig. 7.3. This pattern arises because there are four possible combinations of the spin-states of the two coupled protons and the local magnetic field at the carbon nucleus will be the sum of the field changes induced by each proton. When the magnetic moment of both protons point upwards, in the direction of B_o, the frequency shift of the resonance line will be $2 \times J/2$ Hz, or J Hz. When the proton spins are both pointing in the opposite direction the shift is $-J$ Hz. When the direction of the proton spins are opposite to each other, the local fields at the carbon cancel, resulting in a zero frequency shift of the carbon spin. The intensity of the lines in the carbon spectrum is proportional to the number of molecules in the sample having one of the four possible proton spin-states. Since the state in which the proton spins point in opposing directions occurs twice as frequently as the other two states, the central line of the triplet will have twice the intensity of the outer lines, giving an observed intensity ratio of 1:2:1, as illustrated in Fig. 7.3.

The coupling between a carbon atom and three equivalent protons, such as in a methyl group ($^{13}CH_3$), can be analyzed in exactly the same way. The change in the

[1]Equivalent protons are generally considered to be a collection of protons that are attached to a single carbon atom and have the same chemical shift. Equivalency is most often a result of free rotation of the group, which averages the local environments of all of the protons.

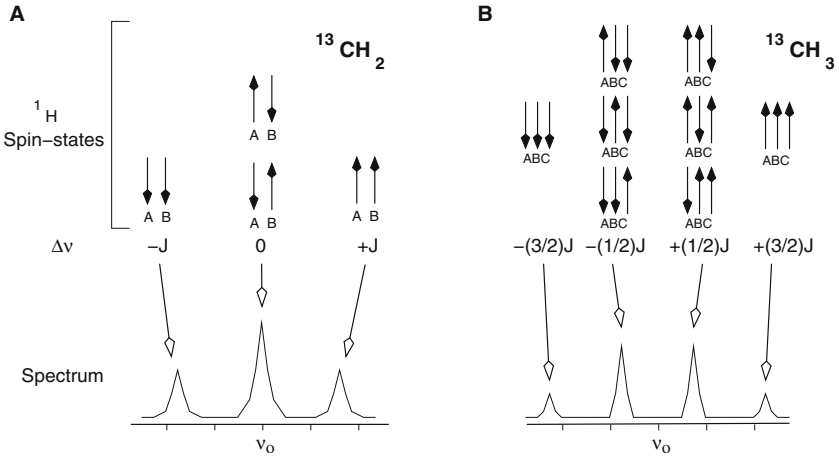

Figure 7.3. Scalar coupling to multiple equivalent protons. The effect of scalar coupling to two (A) or three (B) equivalent protons on the carbon spectrum is shown. The possible arrangements of two (labeled A B) or three protons (labeled A B C) are shown in the upper part of each panel (^{1}H spin-states). The resultant shift in the frequency of the attached carbon is indicated by $\Delta\nu$. The final carbon spectrum is shown in the lower part of each panel. In both cases the splitting, or separation between the lines, is equal to $^1J_{CH}$. The intensity of each line depends on the number of molecules in the sample with a particular spin state; a 1:2:1 ratio will be found for two coupled protons and a 1:3:3:1 ratio is found for three coupled protons.

local field that occurs when the magnetic dipoles from all of the protons are aligned in the same direction is $\pm\frac{3}{2}J$. When the magnetic dipoles of two protons are oriented in the same direction, while the third is pointing in the opposite direction, the frequency shift is $\pm\frac{1}{2}J$ since the opposing pairs cancel each other's effect on the local magnetic field at the carbon nucleus. Again, the relative intensity of each line is proportional to the number of atoms that give a particular frequency shift, in this case the four lines in the quartet will have a relative intensities of 1:3:3:1.

Homonuclear, proton-proton, couplings are analyzed in a similar way. For example, consider the NMR spectrum of ethanol, shown in Fig. 2.6. In this example, all of the carbons are ^{12}C and are therefore NMR inactive. The two CH_2 protons are split into a quartet by the three equivalent methyl protons. Likewise, the three methyl protons are split into a triplet due to coupling to the two equivalent CH_2 protons.

The effect of coupling to multiple spins on an NMR spectral line can be easily obtained from Pascal's triangle, as illustrated in Fig. 7.4. Each row of the triangle

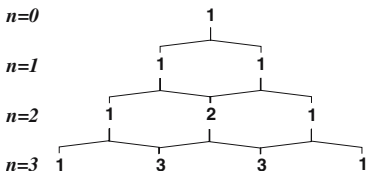

Figure 7.4 Analysis of J-coupling using Pascal's triangle. Pascal's triangle can be used to readily evaluate the effect of coupling to multiple equivalent spins on the appearance of a resonance line. The top of the triangle represents the resonance line from a spin with no coupling partner ($n = 0$) and each subsequent row represents the spectra that would be obtained as a result of coupling to one, two, or three additional spins.

indicates the location of each line in the multiplet as well as the relative intensity of the line.

In cases where an atom is coupled to two different, or non-equivalent, spins, then the couplings are treated independently. For example, the carbonyl carbon is coupled to both the amide nitrogen (${}^1J_{NC'} \approx 12$ Hz) as well as the alpha carbon, (${}^1J_{C'C_\alpha} \approx 55$ Hz), consequently the spectra line from the carbonyl will be a quartet, showing both couplings (see Fig. 7.5).

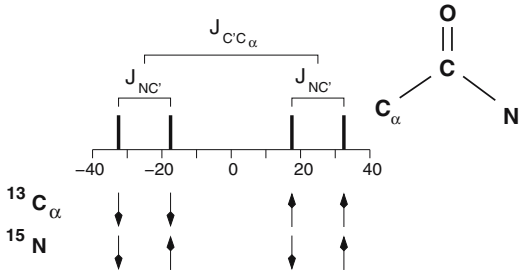

Figure 7.5 Scalar coupling to non-equivalent spins. The spectrum of a carbonyl carbon is shown. A quartet is observed because the coupling to the alpha carbon (J_{CC_α}) is larger than the two bond coupling to the nitrogen (J_{NC}). The spin-states of the C_α carbon and nitrogen are shown below the spectrum. Since these four states are equally likely, the ratio of the intensities of the lines in the quartet are 1:1:1:1.

7.3 Quantum Mechanical Description

The Hamiltonian that describes scalar coupling between spins is given by:

$$\mathcal{H} = \vec{I}\ \tilde{J}\ \vec{S} \tag{7.3}$$

The scalar coupling is represented by a tensor quantity[2] which will be diagonal in some coordinate frame:

$$\tilde{J} = \begin{bmatrix} J_{xx} & 0 & 0 \\ 0 & J_{yy} & 0 \\ 0 & 0 & J_{zz} \end{bmatrix} \tag{7.4}$$

Usually, the different elements are averaged by isotropic rotation in solution, given an observed average value which is a scalar:

$$< J >= \frac{1}{3}[J_{xx} + J_{yy} + J_{zz}] \tag{7.5}$$

This simplifies the Hamiltonian to:

$$\mathcal{H} = J\vec{I} \cdot \vec{J} \tag{7.6}$$

7.3.1 Analysis of an AX System

The dot product, $\vec{I} \cdot \vec{S}$, expands to:

$$I \cdot S = I_x S_x + I_y S_y + I_z S_z \tag{7.7}$$

[2] See Appendix B for a comparison of scalars, vectors, and tensors.

In general, it would be necessary to use the complete expression for the dot product when analyzing the effect of the coupling on the energy states. However, if the frequency difference between the coupled spins is larger than the J-coupling, as is the case in an AX spin-system, then terms involving transverse operators can be dropped. This leads to a simplified representation of the Hamiltonian for a pair of coupled spins:

$$\mathcal{H} = -\omega_I I_z - \omega_S S_z + 2\pi J I_z S_z \tag{7.8}$$

or in frequency units:

$$\mathcal{H} = -\nu_I I_z - \nu_S S_z + J I_z S_z \tag{7.9}$$

Before using this Hamiltonian to calculate the energy levels of the system it is necessary to write expressions for the basis states of the system. Four new states are generated by taking all possible combinations of the original basis vectors that were associated with each spin. These states are[3]:

$$\phi_1 = |\alpha\alpha> \quad \phi_2 = |\beta\alpha> \quad \phi_3 = |\alpha\beta> \quad \phi_4 = |\beta\beta> \tag{7.10}$$

These wavefunctions are eigenfunctions of the *uncoupled* Hamiltonian. The first character (α or β) refers to the I spin while the second character refers to the S spin. In both cases α is associated with an m_z of +1/2, and β is associated with an m_z of -1/2. For example, $|\alpha\beta>$ is a wavefunction in which the I spin has an m_z value of +1/2 and the S spin has an m_z value of -1/2. The four basis states form an ortho-normal basis set, e.g. $<\alpha\alpha|\alpha\alpha>= 1, \ <\alpha\alpha|\alpha\beta>= 0$.

The energy of each of these states is calculated directly from the Hamiltonian ($\mathcal{H}|\Psi>= E_\Psi|\Psi>$):

$$\begin{aligned}
\mathcal{H}|\phi_1> &= -\nu_I/2 - \nu_S/2 + J/4|\alpha\alpha> & (7.11)\\
\mathcal{H}|\phi_2> &= +\nu_I/2 - \nu_S/2 - J/4|\beta\alpha> & (7.12)\\
\mathcal{H}|\phi_3> &= -\nu_I/2 + \nu_S/2 - J/4|\alpha\beta> & (7.13)\\
\mathcal{H}|\phi_4> &= +\nu_I/2 + \nu_S/2 + J/4|\beta\beta> & (7.14)
\end{aligned}$$

The four energy levels are illustrated in Fig. 7.6. Six different transitions are possible with this system. Observable transitions are those that have a non-zero value for the scalar product of the ground and excited state with $I_x + S_x$. The actual probability that the transition will occur is given by the square of the scalar product:

$$P_{g\to e} = |<\psi_e|I_x + S_x|\psi_g>|^2 \tag{7.15}$$

Of the six possible transitions, the following four are observable with equal intensity, with the indicated energies:

[3]Normally, the convention would be to write these states as: $\phi_2 = |\alpha\beta>, \phi_3 = \beta\alpha>$, however, the order used here facilitates solving an AB coupled system, as described in Section 7.3.2.

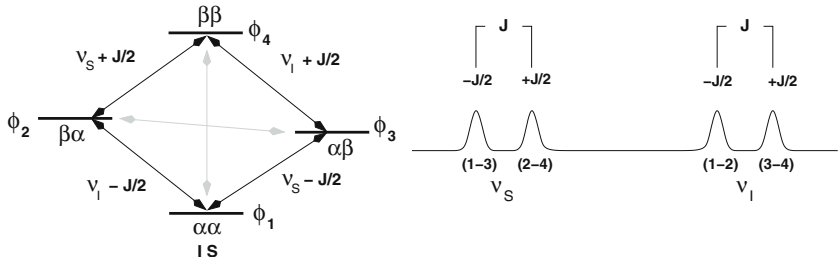

Figure 7.6. Energy levels and resultant spectrum for two coupled spins. The energy level diagram on the left shows the relative energy of all four states. The observable single quantum transitions are indicated by black arrows and the observed frequency of these transitions, in Hz, are also given. Unobservable zero- and double-quantum transitions are indicated with the gray arrows. The right side of the diagram gives the resultant spectrum. The two states that are involved in each transition are indicated underneath each peak. For example, the left-most peak arises from a transition between ϕ_1 and ϕ_3.

$$E_{1\to 2} = \nu_I - J/2 \tag{7.16}$$
$$E_{1\to 3} = \nu_S - J/2 \tag{7.17}$$
$$E_{2\to 4} = \nu_S + J/2 \tag{7.18}$$
$$E_{3\to 4} = \nu_I + J/2 \tag{7.19}$$

These transitions represent a normal 1D NMR spectrum between two coupled spins, as shown in Fig. 7.6.

In addition to the above single quantum transitions there is also a double quantum transition: $E_{\alpha\alpha\to\beta\beta} = \omega_I + \omega_S$, and a zero quantum transition: $E_{\alpha\beta\to\beta\alpha} = \omega_I - \omega_S$, neither of which are directly observable since they involve an overall change in m_z of ± 2 or zero.

7.3.2 Analysis of an AB system

When the chemical shift difference between the two coupled spins is of the same order as the coupling constant it is then necessary to perform a more complete quantum mechanical treatment. This analysis will show that the original eigenstates of the coupled spins are no longer eigenstates of the complete Hamiltonian. It will be necessary to find new eigenstates and eigenvalues (energies) of the system. A remarkable outcome of this analysis is that for the case of completely equivalent spins, such as the protons in a -CH_3 group, the proton-proton coupling vanishes and the quartet collapses into a single line.

We will begin by writing the complete Hamiltonian (in frequency units):

$$\mathcal{H} = -\nu_I I_z - \nu_s S_z + J(I_x S_x + I_y S_y + I_z S_z) \tag{7.20}$$

It is very useful to replace the transverse spin operators (e.g. I_x) by raising and lowering operators:

$$I_x = \frac{1}{2}(I^+ + I^-) \qquad I_y = \frac{1}{2i}(I^+ - I^-) \tag{7.21}$$

$$\begin{aligned} I_x S_x + I_y S_y &= \frac{1}{4}(I^+S^+ + I^+S^- + I^-S^+ + I^-S^-) \\ &\quad -\frac{1}{4}(I^+S^+ - I^+S^- - I^-S^+ + I^-S^-) \\ &= \frac{1}{2}[I^+S^- + I^-S^+] \end{aligned} \tag{7.22}$$

The Hamiltonian has the following form using the previous basis vectors:

$$\begin{array}{rcccc} & |\alpha\alpha> & |\beta\alpha> & |\alpha\beta> & |\beta\beta> \\ <\alpha\alpha| & -\sum\nu/2 + J/4 & 0 & 0 & 0 \\ \mathcal{H} = <\beta\alpha| & 0 & \Delta\nu/2 - J/4 & J/2 & 0 \\ <\alpha\beta| & 0 & J/2 & -\Delta\nu/2 - J/4 & 0 \\ <\beta\beta| & 0 & 0 & 0 & +\sum\nu/2 + J/4 \end{array} \tag{7.23}$$

where $\Delta\nu = \nu_I - \nu_S$ and $\sum\nu = \nu_I + \nu_S$.

The wavefunctions $|\alpha\alpha>$ and $|\beta\beta>$ are still eigenvectors of the complete Hamiltonian since the off-diagonal elements are all zero for these two wavefunctions. In contrast, the $|\alpha\beta>$ and $|\beta\alpha>$ wavefunctions have become mixed by the coupling. It is necessary to find a linear combination of these two functions that are eigenvectors of the complete Hamiltonian. These are obtained by finding the eigenvalues and eigenvectors of the central part of the above matrix (See Cohen-Tannoudji *et al.*[42] for an excellent description of the diagonization of 2x2 matrices. Their results are summarized in this discussion.):

$$\begin{array}{rcc} & |\beta\alpha> & |\alpha\beta> \\ <\beta\alpha| & \Delta\nu/2 - J/4 & J/2 \\ <\alpha\beta| & J/2 & -\Delta\nu/2 - J/4 \end{array} \tag{7.24}$$

The eigenvalues are found by solving the characteristic equation, and they are found to be:

$$E_2 = -\frac{J}{4} + \frac{1}{2}\sqrt{\Delta\nu^2 + J^2} \qquad E_3 = -\frac{J}{4} - \frac{1}{2}\sqrt{\Delta\nu^2 + J^2} \tag{7.25}$$

Finding the eigenvectors of the Hamiltonian is equivalent to finding the rotation that will diagonalize the Hamiltonian. It is convenient to define the rotation angle θ as:

$$tan\theta = \frac{J}{\Delta\nu} \tag{7.26}$$

where $\theta = 0$ when $\Delta\nu >> J$ and $\theta = \pi/2$ when $\Delta\nu << J$.

The eigenvectors, expressed as linear combinations of the original eigenvectors, are:

$$\phi_2 = cos\frac{\theta}{2}|\beta\alpha> + sin\frac{\theta}{2}|\alpha\beta> \qquad \phi_3 = -sin\frac{\theta}{2}|\beta\alpha> + cos\frac{\theta}{2}|\alpha\beta> \tag{7.27}$$

Table 7.2. Observed transitions for two AB coupled spins.

Transition	*Energy*	*Intensity*
$1 \rightarrow 2$	$\bar{\nu} + \frac{1}{2}\sqrt{\Delta\nu^2 + J^2} - \frac{1}{2}J$	$\frac{1}{4}(1 + sin\theta)$
$1 \rightarrow 3$	$\bar{\nu} - \frac{1}{2}\sqrt{\Delta\nu^2 + J^2} - \frac{1}{2}J$	$\frac{1}{4}(1 - sin\theta)$
$2 \rightarrow 4$	$\bar{\nu} - \frac{1}{2}\sqrt{\Delta\nu^2 + J^2} + \frac{1}{2}J$	$\frac{1}{4}(1 + sin\theta)$
$3 \rightarrow 4$	$\bar{\nu} + \frac{1}{2}\sqrt{\Delta\nu^2 + J^2} + \frac{1}{2}J$	$\frac{1}{4}(1 - sin\theta)$

$\bar{\nu} = (\nu_I + \nu_S)/2$ is the frequency at the center of the quartet.

The four observable transitions, their energies and intensities, are shown in Table 7.2. The transition probabilities are calculated as described in Eq. 7.15. For example, the probability of the $2 \rightarrow 1$ transition is obtained as follows:

$$\begin{aligned} P_{2-1} &= | < \phi_1 | I_x + S_x | \phi_2 > |^2 \\ &= | < \alpha\alpha | I_x + S_x | \left[cos\frac{\theta}{2}|\beta\alpha > + sin\frac{\theta}{2}|\alpha\beta > \right] |^2 \\ &= \frac{1}{4}| < \alpha\alpha | I^+ + I^- + S^+ + S^- | \left[cos\frac{\theta}{2}|\beta\alpha > + sin\frac{\theta}{2}|\alpha\beta > \right] |^2 \\ &= \frac{1}{4}| < \alpha\alpha | \left[sin\frac{\theta}{2}|\beta\beta > + cos\frac{\theta}{2}|\alpha\alpha > + cos\frac{\theta}{2}|\beta\beta > + sin\frac{\theta}{2}|\alpha\alpha > \right] |^2 \\ &= \frac{1}{4}| \left[cos\frac{\theta}{2} + sin\frac{\theta}{2} \right] |^2 \\ &= \frac{1}{4}(1 + sin\theta) \end{aligned} \tag{7.28}$$

The effect of the frequency separation between the coupled spins on the appearance of the spectra is shown in Fig. 7.7. In this simulation the J-coupling constant was 10 Hz, a typical value for proton-proton couplings in amino acids. The lower curve shows the expected spectra for a frequency separation of 100 Hz, or 0.2 ppm on a 500 MHz spectrometer. Although $\Delta\nu = 10J$, some effects of the mixing of the states are

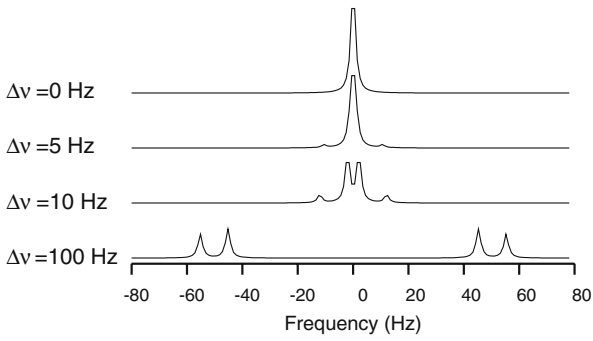

Figure 7.7 Effect of frequency separation on observed J-coupling. Simulated spectra are shown to illustrate the collapse of observed coupling as $\Delta\nu$ becomes smaller than J. The J-coupling constant is 10 Hz, and the separation between the lines is decreased from 100 Hz (bottom spectrum) to 0 Hz (top spectrum).

already apparent. The outer transitions show a lower intensity and the positions of the lines are shifted by a few 10^{ths} of a Hertz. As the frequency separation between the two coupled spins decreases, the intensity of the outer lines decreases and the lines move towards the average frequency. Finally, when the spins are equivalent ($\nu_I = \nu_S$; $\Delta\nu = 0$), there is no observable coupling.

7.4 Decoupling

Scalar coupling leads to splitting of spectra lines and therefore reduces the signal-to-noise in the spectrum by spreading the intensity over all of the peaks in the multiplet. This loss in signal-to-noise can be restored by collapsing the multiplet to a single line by *decoupling*. Since the splitting arises from the influence of the magnetic state of one spin on the other, decoupling can be accomplished by simply inverting the spin-state of the coupled partner during detection. For example, in the case of a ^{13}CH group, if the carbon magnetization is inverted rapidly, the protons in the sample no longer sense two distinct carbon spin-states, but a single averaged state. One way of achieving this inversion is to simply apply a train of 180° pulses to the carbon, as illustrated in Fig. 7.8. More effective decoupling is obtained as the rate of inversion is increased by reducing both the inter-pulse spacing and the 180° pulse length.

7.4.1 Experimental Implementation of Decoupling

Decoupling is incorporated into one-dimensional proton NMR experiments as illustrated in Fig. 7.9. In the case of proton decoupling during proton acquisition it is necessary to gate the decoupling off during digitization of the data, otherwise the decoupling pulses would enter the receiver. In the case of heteronuclear decoupling, it is possible to decouple the *non*-observed spin continuously while acquiring the proton signal.

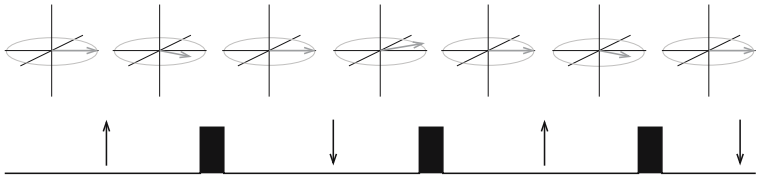

Figure 7.8. Averaging of spin states during decoupling. A series of π pulses can average spin states, removing the effects of spin-spin scalar coupling on the NMR spectrum (decoupling). The upper part of the figure shows the precession of a *single* proton in a CH or NH group. The lower segment shows a train of π pulses that are applied to the heteronuclear spin (^{13}C or ^{15}N). The black vertical arrows represent the spins state of the heteronuclear spin. The proton originally precesses in a clockwise direction. Inversion of the heteronuclear spin reverses the direction. If the inter-pulse delay is small compared to the J-coupling, the proton simply oscillates around the y-axis without undergoing any evolution due to J-coupling. Consequently its position in the spectrum is defined solely by its chemical shift and no splitting of the line occurs.

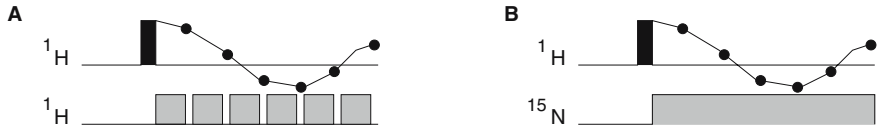

Figure 7.9. Decoupling in one-dimensional pulse sequences. The experimental set-up for homonuclear (A) and heteronuclear (B) decoupling are shown. In the case of heteronuclear decoupling a separate radio-frequency channel is required for the heteronuclear spin. In contrast, homonuclear ^{1}H-^{1}H decoupling would utilize the same circuit as the excitation pulse. The top part of each panel shows a standard one-dimensional pulse sequence and resultant FID, sampled at the times indicated by the filled circles. The lower part shows the decoupling pulses, as gray rectangles. Homonuclear decoupling is gated, or turned off, during digitization of each point, otherwise the intense decoupling power would corrupt the signal. In the case of heteronuclear decoupling, the pulses can be applied continuously because the decoupling enters the probe on a completely separate circuit, hence little power is transferred to the proton detection channel. In addition, the large frequency difference between the detected proton signal (e.g. 500 MHz) versus that of the decoupling pulse (e.g. 50 MHz) facilitates removal of the decoupling signal by filtering.

7.4.2 Decoupling Methods

Due to resonance off-set effects, the simple inversion of the coupled partner by the application of 180° pulses is very ineffective if the resonance frequency of the decoupled spin differs from the carrier frequency. Because of the wide frequency range of ^{13}C and ^{15}N spins it has been necessary to design more elaborate pulse sequences for decoupling of these nuclei.

Decoupling schemes can be divided into two broad categories, those which were designed for isolated X-H systems, where there are no other significant couplings, and those that were designed for systems where the coupled partner shows coupling to atoms of the same type. An example of the former is the NH group, where the ^{15}N has no other coupling partners except for the amide proton. An example of the latter is the $C_\alpha H_2$ group in glycine. The two α-protons show strong proton-proton coupling, on the order of 15 Hz, that can interfere with proton decoupling during the observation of carbon.

The three commonly used decoupling schemes for isolated H-C and H-N spins are MLEV-16, WALTZ-16, and GARP-1. These schemes are usually provided with the software that accompanies the spectrometer or are easily programmed with the pulse program software. A detailed description of the development and properties of these schemes can be found in Freeman [56]. MLEV-16 is an early decoupling scheme whose properties are inferior to WALTZ and GARP and is only included here for purposes of comparison.

The schemes that have been designed for the decoupling of scalar coupled spins consist of a collection of three related schemes: DIPSI-1, DIPSI-2, and DIPSI-3 (Decoupling In the Presense of Scalar Interations). The basic pulse elements that make up each of the DIPSI sequences, along with an indication of their performance levels are presented in Table 7.3. The three DIPSI sequences differ in the length of the fundamental rotation operator (see below) to accommodate timing limitations that

may occur in pulse sequences. DIPSI-1 is the shortest sequence and comparable to WALTZ-16 in overall length.

Each of these decoupling schemes are composed of a fundamental rotation operator, R, which is applied with various phases during decoupling. Each rotation operator, R, can be considered to be equivalent to a 180° pulse, causing inversion of the decoupled spin. In these decoupling schemes the rotation operators have been designed to be insensitive to resonance offset effects. The MLEV rotation operator is one of the simplest; a composite 180° pulse (see Sec. 6.3.3, pg. 132). The different rotation operators associated with each decoupling scheme are shown in Table 7.3. Additional insensitivity to resonance offset effects is obtained by forming a four element cycle of the basic rotation operator:

$$RR\bar{R}\bar{R} \tag{7.29}$$

where $\bar{R}$ is the inverse of R. In the case of MLEV and WALTZ decoupling, cyclic permutations of this basic cycle are combined to give a 16 step super-cycle,

$$RR\bar{R}\bar{R}\ \ \bar{R}RR\bar{R}\ \ \bar{R}\bar{R}RR\ \ R\bar{R}\bar{R}R \tag{7.30}$$

which further compensates for resonance-offset effects. The number of R elements in the super-cycle are often indicated in name of the decoupling scheme, e.g. MLEV-4=$RR\bar{R}\bar{R}$ and MLEV-16=$RR\bar{R}\bar{R}\ \ \bar{R}RR\bar{R}\ \ \bar{R}\bar{R}RR\ \ R\bar{R}\bar{R}R$.

Decoupling Scheme	*R Element*	Ξ	*Residual Line Broadening*	*Ref.*
MLEV-16	$[\pi/2]_x[\pi]_y[\pi/2]_x$	1.5	Large	[94]
WALTZ-16	$[\pi/2]_x[\pi]_{-x}[3\pi/2]_x$	1.8	Small	[147]
DISPI-1	$365\ \overline{295}\ 65\ \overline{305}\ 350$	0.8	Small	[148]
DISPI-2	$320\ \overline{410}\ 290\ \overline{285}\ 30\ \overline{245}\ 375\ \overline{265}\ 370$	1.2	Small	[148]
DISPI-3	$\overline{245}\ 395\ \overline{250}\ 275\ \overline{30}\ 230\ \overline{360}\ 245\ \overline{370}\ 340$ $\overline{350}\ 260\ \overline{270}\ 30\ \overline{225}\ 365\ \overline{255}\ 395$	1.6	Very Small	[148]
GARP-1	$R = \bar{P}Q\overline{PQ}$, overall cycle is $RR\bar{R}\bar{R}$ $P = 27.1\ \overline{57.6}\ 122.0$ $Q = \overline{120.8}\ 262.8\ \overline{65.9}\ 64.6$ $\overline{87.0}\ 90.0\ \overline{137.2}\ 256.2\ \overline{71.6}\ 51.1$	4.8	Moderate	[146]

Table 7.3. Decoupling schemes. The properties of a number of common decoupling schemes are shown. The R element is the basic rotation operator that is used to form the $RR\overline{RR}$ decoupling element. Pulse angles and phases are indicated. In the case of DIPSI and GARP decoupling, the pulses are along the x-axis or along the minus x-axis if the angle is overlined. Angles are given in degrees. The figure of merit, Ξ, for each sequence is also provided. Finally, the quality of the decoupling is indicated by the residual line broadening; higher quality sequences have a smaller residual line broadening.

7.4.3 Performance of Decoupling Schemes

The frequency range over which the decoupling is effective is characterized by the *bandwidth*. Empirically, decoupling is considered to be effective if the intensity of the collapsed multiplet has at least 80% of the intensity of the fully decoupled signal. The bandwidth can be increased by using shorter pulses in the decoupling sequence. However, the additional power will cause sample heating, and in extreme cases can lead to equipment failure. Since the decoupling bandwidth is proportional to the field strength of the decoupling pulses, it is convenient to define a figure of merit, Ξ, as:

$$\Xi = \frac{2\pi\Delta F}{\gamma B} \tag{7.31}$$

where ΔF is the region over which the decoupling is effective (in Hz), and γB is the strength of the decoupling field (in units of rad/sec). Schemes that have a higher figure of merit can decouple a larger bandwidth for the same amount of RF power.

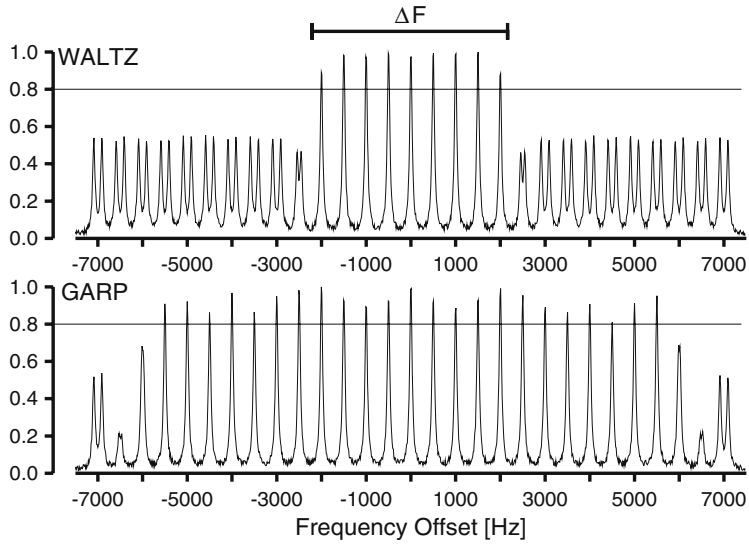

Figure 7.10. Bandwidth of WALTZ and GARP decoupling. A series of NMR spectra of a single amide proton, attached to an ^{15}N spin, are shown for different decoupler frequencies. The decoupler frequency is given relative to the frequency of the ^{15}N resonance. This frequency was varied in 500 Hz steps, ranging from 7000 Hz below (left) to 7000 Hz above the nitrogen frequency (right). A single line indicates collapse of the proton doublet to a singlet. For frequencies far outside the bandwidth, a doublet is observed, with a splitting of 92 Hz ($J_{NH} = 92$ Hz). The horizontal line marks a relative height of 0.8 for the proton line, defining the bandwidth. Outside the bandwidth, the residual linewidth broadens the line, decreasing the signal height. In this illustration the bandwidth of the WALTZ decoupling is 4 kHz, while that for GARP decoupling is 11 kHz. In the case of GARP decoupling, the height of the proton lines are not uniform within the bandwidth due to a variation in the residual decoupling that depends on the frequency offset. In contrast, the height of the lines for WALTZ decoupling are uniform, indicating a small dependence of the residual coupling on the frequency offset.

The Ξ values for MLEV-16, WALTZ-16, DIPSI-*n*, and GARP-1 decoupling are shown in Table 7.3. MLEV-16 has the smallest bandwidth while WALTZ-16 has a slightly larger bandwidth, but the quality of the decoupling is much higher (see below). GARP-1 has the largest bandwidth of the three schemes, but is of lower quality than WALTZ-16. The bandwidths of the DIPSI-*n* sequences depend on the length of the sequence with DIPSI-3 providing the largest bandwidth of the three. However, its bandwidth is still smaller than that of WALTZ-16.

In addition to differing in bandwidth, decoupling schemes also differ in the amount of residual coupling that remains in effect in the presence of the decoupling. The residual coupling will increase the apparent linewidth of the unresolved multiplet, causing a decrease the intensity of the observed peak. The amount of residual coupling depends on the decoupling scheme (see Table 7.3 and Fig. 7.10). In the case of H-X decoupling schemes, WALTZ-16 has a much smaller residual bandwidth than GARP or MLEV-16, and therefore gives high quality decoupling. Of the DIPSI decoupling schemes, DIPSI-3 produces excellent decoupling in the case of scalar coupled systems, out-performing WALTZ-16. A guide to the selection of decoupling schemes is given in Table 7.4

Table 7.4. Guide to decoupling schemes.

Situation	*Decoupling Scheme*	*Rational*
Decouple ^{15}N, observe protons.	WALTZ-16.	Narrow bandwidth of ^{15}N, typically 30 ppm (ΔF = 1.8 kHz) with no ^{15}N-^{15}N coupling, WALTZ-16 provides excellent line-narrowing.
Decouple ^{13}C, observe protons.	GARP-1 for natural abundance.	Require high bandwidth to cover carbon spectrum. Typical bandwidth is 80 ppm ($\Delta F = 12$ kHz).
	DIPSI-3 for uniformly labeled samples, provided sufficient bandwidth can be generated. This will depend on the hardware and the desired bandwidth.	^{13}C-^{13}C couplings can interfere with GARP-1 decoupling.
Decouple ^{1}H, observe carbon or nitrogen.	DISPI-2 or DIPSI-3. Timing constraints may force the use of DIPSI-2 in triple resonance experiments.	Moderate proton bandwidth needed, 4 ppm ($\Delta F = 2.4$ kHz) for amides, 6 ppm for aliphatics ($\Delta F = 3.6$ kHz). ^{1}H-^{1}H couplings will interfere with WALTZ-16 and GARP-1.

7.5 Exercises

1. What was the power of the decoupler field strength, in units of Hz, for the series of spectra that were shown in Fig. 7.10?

2. The ^{15}N chemical shift of amide groups range from 100 to 135 ppm. Assuming a magnetic field strength that gives a proton frequency 500 MHz, would WALTZ decoupling at the decoupler power level used in Fig. 7.10 provide satisfactory decoupling?

3. What *change* in power level would be required to adjust the bandwidth of the WALTZ decoupling in Fig. 7.10 to 1750 Hz.

4. Aliphatic carbon frequencies range from 0 to 70 ppm. Assuming a magnetic field strength that gives a proton frequency of 800 MHz, calculate the decoupler field strength required to decouple this bandwidth using WALTZ decoupling. What is the equivalent 90° pulse width for this field strength? Is is possible to use WALTZ decoupling to decouple carbons at this field strength?

5. Given that the 90° pulse length for ^{15}N spin is 40 μsec at a power level of 0 dB, calculate the power required to decouple over a bandwidth of 1800 Hz using WALTZ decoupling.

7.6 Solutions

1 The bandwidth for WALTZ decoupling was 4 kHz. The figure of merit for WALTZ is 1.8, $\Xi = 2\pi\Delta F/\gamma B$, therefore:

$$\begin{aligned} 1.8 &= \frac{2\pi 4000}{\gamma B} \\ \gamma B &= \frac{2\pi 4000}{1.8} \\ &= 13,962 \text{ rad/sec} = 2,222 \text{ Hz} \end{aligned}$$

2 A 35 ppm ^{15}N chemical shift range corresponds to 1750 Hz at this magnetic field strength. The 4 kHz bandwidth will be more than adequate.

3 This requires a reduction in the decoupler field strength by a factor of 2.3 (4,000/1,750). Therefore the attenuation will be:

$$\begin{aligned} \text{dB} &= 20\, log \frac{V_1}{V_2} \\ &= 20\, log\, 2.3 \\ &= 7.18 \end{aligned}$$

4 A 70 ppm is equivalent to 14 kHz (70 ppm x 200 MHz). Given a figure of merit of 1.8 for WALTZ decoupling, a decoupler field strength of approximately 7,800 Hz is required. At this field strength, a 90° pulse would require 32 μsec. This

pulse length is close to the length that would be considered at full power. Hence WALTZ decoupling of carbon at this magnetic field strength would certainly lead to sample heating and would likely result in equipment failure.

5 The figure of merit for WALTZ is 1.8, therefore a 1 kHz decoupler field strength would be sufficient. The field strength at 0 dB can be obtained from the 90° pulse length:

$$\begin{aligned} \gamma B_1[\mathrm{Hz}] &= \frac{1}{4\tau} \\ &= 6250\ \mathrm{Hz} \end{aligned}$$

The change in power is calculated as follows:

$$\mathrm{dB} = 20\ log\frac{1000}{6250} = 20 \times (-0.795) = -15.9\ \mathrm{dB}. \tag{7.32}$$

Therefore, the power level should be decreased by 15.9 dB.